

Unparticle Self-Interactions at the Large Hadron Collider

Johannes Bergström* and Tommy Ohlsson†

*Department of Theoretical Physics, School of Engineering Sciences,
Royal Institute of Technology (KTH) – AlbaNova University Center,
Roslagstullsbacken 21, 106 91 Stockholm, Sweden*

(Dated: November 1, 2018)

Abstract

We investigate the effect of unparticle self-interactions at the Large Hadron Collider (LHC). Especially, we discuss the three-point correlation function, which is determined by conformal symmetry up to a constant, and study its relation to processes with four-particle final states. These processes could be used as a favorable way to look for unparticle physics, and for weak enough couplings to the Standard Model, even the only way. We find updated upper bounds on the cross sections for unparticle-mediated 4γ final states at the LHC and novel upper bounds for the corresponding $2\gamma 2\ell$ and 4ℓ final states. The size of the allowed cross sections obtained are comparably large for large values of the scaling dimension of the unparticle sector, but they decrease with decreasing values of this parameter. In addition, we present relevant distributions for the different final states, enabling the possible identification of the unparticle scaling dimension if there was to be a large number of events of such final states at the LHC.

PACS numbers: 12.60.-i; 13.85.-t; 14.80.-j

*Electronic address: johbergs@kth.se

†Electronic address: tommy@theophys.kth.se

I. INTRODUCTION

The Standard Model (SM) of particle physics has to date been extremely successful yielding consistent results and most accurate predicting properties of particles and their interactions. However, in its minimal version, it does not contain massive neutrinos, gravity, and/or dark matter. Although it should be fairly easy to include massive neutrinos as well as neutrino oscillations in a minimally extended version of the SM, one of the most important particles of the SM has not yet been experimentally confirmed, namely the Higgs boson, which is responsible for giving masses to the particles of the SM. Therefore, the Large Hadron Collider (LHC) has been constructed and will hopefully be able to discover it. In the connection with the process of constructing the LHC, a lot of alternative pictures have been proposed, including for example unparticle physics that was introduced by Howard Georgi in 2007 [1]. Thus, in the last couple of years, several studies of the phenomenology of unparticle physics have appeared in the literature. In this work, we will focus on studying the effects of unparticle self-interactions at colliders, and especially the LHC. In general, our investigation will be based on the unparticle three-point correlation function, and in particular, we will discuss the phenomenology of unparticle self-interactions in processes with different four-particle final states such as four photons (4γ), two photons and two charged leptons ($2\gamma 2\ell$), and four charged leptons (4ℓ) as well as final states including neutrinos, i.e., $2\gamma\nu\bar{\nu}$ and $2\ell\nu\bar{\nu}$.

Previously, an investigation of unparticle self-interactions that is of great importance for this work has been presented in the following paper: In Ref. [2], collider signals of unparticle self-interactions especially with four-photon final states are investigated, which lead to upper bounds on cross sections using Tevatron data that follow from restricting the unparticle self-interactions. In addition, Strassler [3] has discussed self-interactions in general and Georgi and Katz [4] have discussed the production of unparticles through the amputated three-point function.

Our work is organized as follows. In Sec. II, we introduce our model based on a conformal hidden sector coupled to the SM and also present the specific couplings to the SM. Then, in Sec. III, we explicitly derive the unparticle three-point correlation function and discuss the general form of the four-point correlation function. Next, in Sec. IV, we present the phenomenology of our model concerning different four-particle final states mediated by the unparticle three-point function at the LHC. By using existing Tevatron data, we constrain

the constant appearing in the three-point function, enabling determination of the maximum allowed cross sections at the LHC. Furthermore, relevant distributions are given, which could be used to identify unparticle physics as a possible interpretation of future data in the event that a large number of events with four-body final states were to be measured at the LHC. Finally, in Sec. V, we give a short summary of our work as well as our main conclusions.

II. THE MODEL

The most famous examples of four-dimensional conformal field theories, which could serve as hidden sectors, are theories of so-called Banks–Zaks type [5]. These are gauge theories with the number of fermions chosen such that an infrared stable fixed point emerges at two loops. In addition, one can have supersymmetric versions of these types of theories and even calculate the fraction of them being conformal in the infrared regime [6].

In general, unitary four-dimensional scale-invariant quantum field theories are also conformally invariant with no known counterexamples [7–9]. Unitarity demands that the scaling dimension of an operator with Lorentz spins j_1 and j_2 is $d \geq j_1 + j_2 + 2 - \delta_{j_1 j_2, 0}$ [10]. This translates into $d_S \geq 1$, $d_{Sp} \geq 3/2$, and $d_V \geq 3$ for Lorentz scalar, spinor, and gauge invariant vector operators, respectively. However, much of the phenomenology of unparticle physics dealing with vector operators are performed for values violating these bounds. One also finds that the fields satisfy equations of motion for free fields and conservation laws if and only if the lower bounds are saturated. For vector operators, this includes the existence of zero-norm descendants $\partial_\mu V^\mu(x) = 0$, which does not hold away from the unitarity bound.

The basic scheme for our model is the following. There is a hidden sector of Banks–Zaks type that couples to the SM through a ‘messenger field’ with a large mass M , which simply means that both the SM and the hidden sector couple to this field. Below the scale M , one can use effective field theory and integrate out the heavy field, whereby one ends up with effective operators suppressed by powers of M on the form¹

$$c_n^i \frac{1}{M^{n+d_{UV}-4}} \mathcal{O}_n^i \mathcal{O}_{UV}, \quad (1)$$

where c_n^i are dimensionless constants and \mathcal{O}_n^i and \mathcal{O}_{UV} are local operators constructed out of the SM and hidden sector fields with mass dimensions n and d_{UV} , respectively. The hidden

¹ Our notation will follow that of Ref. [11].

sector becomes conformal at the scale $\Lambda_{\mathcal{U}}$,² for example, by quantum effects via dimensional transmutation. The operator \mathcal{O}_{UV} changes into $\Lambda_{\mathcal{U}}^{d_{UV}-d}\mathcal{O}_{\mathcal{U}}$, where $\mathcal{O}_{\mathcal{U}}$ has scaling and mass dimension d . This implies that the couplings in Eq. (1) have to be replaced by

$$c_n^i \frac{\Lambda_{\mathcal{U}}^{d_{UV}-d}}{M^{n+d_{UV}-4}} \mathcal{O}_n^i \mathcal{O}_{\mathcal{U}} = c_n^i \frac{1}{\Lambda_n^{n+d-4}} \mathcal{O}_n^i \mathcal{O}_{\mathcal{U}}, \quad (2)$$

where the effective scale Λ_n is given by

$$\Lambda_n^{n+d-4} = \frac{M^{n+d_{UV}-4}}{\Lambda_{\mathcal{U}}^{d_{UV}-d}}. \quad (3)$$

Note that M , $\Lambda_{\mathcal{U}}$, d , and d_{UV} are parameters of the messenger and hidden sector, while n will depend on what SM operator is under consideration. Thus, Λ_n will depend on n (and hence the subscript), i.e., operators of different mass dimension will couple with different strengths. In fact, these different energy scales counteract the effective field theory intuition that higher-dimensional operators are more highly suppressed [11]. In addition, note that the elimination of the heavy field induces contact interactions between generic SM fields such as

$$\mathcal{O}_n^i \mathcal{O}_{n'}^{i'}, \mathcal{O}_n^i \partial^2 \mathcal{O}_{n'}^{i'}, \dots,$$

suppressed by powers of M . These interactions have the potential to drown any unparticle effects [7], at least for values of d much larger than 1, and thus could give the most stringent constraints on the parameter space relevant for unparticle physics.

Since the scaling dimension of the scalar unparticle operator exceeds one and all the SM operators except one that it can couple to all have mass dimension $n \geq 3$, these couplings are all irrelevant. The only coupling that can possibly be relevant is the Higgs-unparticle coupling

$$\frac{\Lambda_{\mathcal{U}}^{d_{UV}-d}}{M^{d_{UV}-2}} H^\dagger H \mathcal{O}_{\mathcal{U}} = \frac{1}{\Lambda_2^{d-2}} H^\dagger H \mathcal{O}_{\mathcal{U}}. \quad (4)$$

For $d < 2$, this coupling is indeed relevant and can significantly alter the low-energy physics of the unparticle sector. Once the Higgs field develops a vacuum expectation value v (giving $H^\dagger H \rightarrow v^2$), this operator introduces a scale into the conformal field theory and will cause the theory to become nonconformal at the energy scale $\Lambda_{\mathcal{U}}$ [12], where

$$\Lambda_{\mathcal{U}}^{4-d} = \Lambda_2^{2-d} v^2. \quad (5)$$

² This scale can for example be defined as the scale, where the coupling has reached $\sqrt{2/3}$ of its fixed-point value.

Below the scale $\Lambda_{\mathcal{U}}$, the hidden sector presumably becomes a conventional particle sector. For consistency, one requires $\Lambda_{\mathcal{H}} \leq \Lambda_{\mathcal{U}}$ and the two scales to be reasonably well separated in order to give a window, where the sector is conformal.

The standard way to treat the breaking of conformal symmetry is to introduce a mass gap in the spectral density. In the absence of fine tuning, this mass gap is at least several GeVs. This implies that there are no long-range forces from unparticle exchange and that precision constraints in practice disappear. Thus, low-energy experiments are not sensitive to unparticle effects, and these are most easily probed at colliders. If the energy of the process in question is high enough, one can simply ignore the mass gap in the expression for the propagator. In Sec. IV, the unparticle three-point function will be used to study possible signals at the LHC. Although it is unclear how to implement the breaking of conformal invariance into this function, it is a reasonable assumption that one can ignore the existence of the mass gap when calculating the three-point function as long as *all* the momentum invariants [q_1^2 , q_2^2 , and $(q_1+q_2)^2$] in the function are much larger than the conformal symmetry breaking scale. Since this will generally be the case at the LHC, this subject will not be discussed any further.

Covariance under conformal transformations determines the (exact) two-point functions of primary scalar operators \mathcal{O}_i with scaling dimensions d_i to be

$$\langle \mathcal{O}_i(x) \mathcal{O}_j(0) \rangle \propto \frac{\delta_{d_i d_j}}{(-x^2 + i\epsilon)^{d_i}} \propto \delta_{d_i d_j} \int \frac{d^4 p}{(2\pi)^4} (-p^2 - i\epsilon)^{d_i - 2} e^{-ip \cdot x}, \quad (6)$$

which give the expressions for the momentum space propagators that can enter in processes with internal unparticle lines. The form of the propagator can give unusual kinematical distributions due to the unusual dependence on p^2 and the unusual phase, i.e., $e^{-i\pi d}$, which can lead to strange interference effects with photon and Z boson propagators [13–15]. Furthermore, the phase space is given by the imaginary part of the propagator

$$d\Phi \propto \theta(P^0) \theta(P^2) (P^2)^{d-2} d^4 P. \quad (7)$$

The real proportionality constant (generally denoted by A_d) corresponds to field normalization and is most commonly chosen such that the phase space interpolates that of d massless particles [1]. The unparticle phase space will enter in processes with an unparticle line in the final state. However, for $d > 2$, it is ultraviolet sensitive and one sometimes finds singular behavior. For example, the energy density at finite temperature and some cross sections are

proportional to $2 - d$ [16, 17]. This together with the lower bound on the scaling dimension from unitarity implies that one usually restricts the attention to the range $1 \leq d \leq 2$ for scalars.

Finally, it is generally assumed that an unparticle does not decay into SM particles. Thus, the unparticle will simply leave any detector undetected and lead to missing energy signals. However, the couplings to SM fields can through loops give a width to the unparticle propagator [18, 19], which means that the unparticle can, depending on model parameters, decay back into SM particles. For an overview of the phenomenology of unparticle physics, see for example Ref. [20] and references therein.

Higher-order processes in the unparticle sector will enter through the unparticle n -point correlation function for $n \geq 3$. Some general ideas can be found in Ref. [3], and in Ref. [4], the production of unparticle stuff through its self-interactions has been studied. In this paper, we will follow Ref. [2] and look at the implications for LHC physics of the unparticle three-point function mediating interactions between SM particles.

A. Couplings to the Standard Model

In order to calculate observables, one needs explicit expressions for the couplings of the unparticle operator to the SM. Initially, the only constraints on the SM operators are that the interaction terms form Lorentz scalars. To reduce the number of possible interactions, one can assume that the unparticle operator is gauge invariant, and thus, the SM operators have to be so as well. All couplings of scalar, spinor, and vector unparticle operators to gauge invariant SM operators with dimensions less than or equal to four have been given in Ref. [21].

For a scalar unparticle field with scaling dimension d , the leading order (in Λ) interaction with SM gauge bosons is through [11]

$$\frac{c_4^F}{\Lambda_4^d} F_{\mu\nu}^a F^{a\mu\nu} \mathcal{O}_U \quad (8)$$

and with fermions after electroweak symmetry breaking through

$$\frac{ec_4^f}{\Lambda_4^d} v \bar{f}_L f_R \mathcal{O}_U + \frac{ec_4^{f_{L,R}}}{\Lambda_4^d} \bar{f}_{L,R} \gamma_\mu f_{L,R} \partial^\mu \mathcal{O}_U, \quad (9)$$

where the electromagnetic coupling has been pulled out for convenience. The first of these two operators is proportional to v . Integrating the second one by parts, the vector contri-

bution vanishes, while the axial-vector contribution is proportional to the fermion mass m_f . Since $m_f \ll v$ for all fermions except the top quark, the first interaction term will dominate for $c_4^f = O(c_4^{fL,R})$. Thus, the Feynman rules for the interactions of photons, gluons, and fermions with a scalar unparticle field are given by

$$\mathcal{O}_{Ugg}, \mathcal{O}_{U\gamma\gamma} \text{ vertex: } \quad i \frac{4c_{g,\gamma}}{\Lambda_4^d} (-p_a \cdot p_b g^{\mu\nu} + p_a^\nu p_b^\mu), \quad (10)$$

$$\mathcal{O}_{U\bar{f}f} \text{ vertex: } \quad i \frac{ec_4^f}{\Lambda_4^d} v P_R, \quad (11)$$

respectively, which will be used to study unparticle phenomenology in the rest of this work.

For primary vectors, the interaction with SM fermions would be through

$$\frac{c_3^{fL,R}}{\Lambda_3^{d-1}} \bar{f}_{L,R} \gamma_\mu f_{L,R} \mathcal{O}_U^\mu, \quad (12)$$

which would not be suppressed as the corresponding operator in Eq. (9). A vector unparticle field cannot couple directly to gauge bosons, since the number of uncontracted Lorentz indices will always be odd. However, it can couple to them through a term like $H^\dagger D_\mu H \mathcal{O}_U^\mu$. A gauge invariant unparticle spinor can only couple in the same way as a right-handed neutrino, and thus, it is possible to replace the ordinary right-handed neutrino with a conformal one [22].

III. THE UNPARTICLE THREE-POINT CORRELATION FUNCTION

In this section, we will investigate the scalar unparticle three-point correlation function. Then, in Sec. IV, we will make use of it to study unparticle self-interactions at the LHC. In general, the three-point function can involve fields with different spins [23], but here we will only consider scalars. The three-point functions of scalar fields \mathcal{O}_i with scaling dimensions d_i are constrained by conformal invariance as

$$\langle \mathcal{O}_1(x_1) \mathcal{O}_2(x_2) \mathcal{O}_3(x_3) \rangle = C_{123} \frac{1}{(x_{12}^2)^{(d_1+d_2-d_3)/2} (x_{23}^2)^{(d_2+d_3-d_1)/2} (x_{13}^2)^{(d_1+d_3-d_2)/2}}, \quad (13)$$

for some constant C_{123} and where $x_{ij} = x_i - x_j$.

To calculate amplitudes, one needs the Fourier transform of the three-point function. This can be performed in a general number of dimensions D and for different values of the scaling dimensions d_i of the three fields, but we will be interested in the case $D = 4$ only

and $\mathcal{O}_1 = \mathcal{O}_2 = \mathcal{O}_u$ and $\mathcal{O}_3 = \mathcal{O}_u^\dagger$, yielding $d_1 = d_2 = d_3 = d$. Then, Eq. (13) gives

$$\Gamma_3(p_1, p_2; d) = C_d \int d^4 x_1 d^4 x_2 \frac{1}{(x_{12}^2)^{d/2} (x_1^2)^{d/2} (x_2^2)^{d/2}} e^{ip_1 \cdot x_1} e^{ip_2 \cdot x_2}, \quad (14)$$

for the Fourier transform of the three-point function, where C_d is a constant. Insertion of the resolution of the identity in the form

$$1 = \int d^4 z \delta^{(4)}[z - (x_1 - x_2)] = \int \frac{d^4 q}{(2\pi)^4} d^4 z e^{-iq \cdot [z - (x_1 - x_2)]}, \quad (15)$$

yields

$$\Gamma_3(p_1, p_2; d) = C_d \int \frac{d^4 q}{(2\pi)^4} \Gamma_2(q; d/2) \Gamma_2(p_1 - q; d/2) \Gamma_2(p_2 + q; d/2), \quad (16)$$

up to an overall d -dependent constant, which is absorbed into C_d . Here $\Gamma_2(k; g) \propto (-k^2 - i\epsilon)^{g-2}$ is the propagator of the scalar field with scaling dimension g as in Eq. (6). Since this resembles a standard loop integral, one can introduce Feynman parameters and end up with the result

$$\Gamma_3(p_1, p_2; d) = -i e^{-i\frac{3d}{2}\pi} C_d \left(\frac{1}{s}\right)^{4-3d/2} T_I(p_1^2/s, p_2^2/s), \quad (17)$$

where

$$T_I(p_1^2/s, p_2^2/s) = \frac{\Gamma(4-3d/2)}{\Gamma(2-d/2)^3} \frac{1}{(4\pi)^2} \int dy_1 dy_2 dy_3 \delta(y_1 + y_2 + y_3 - 1) \times \left(\frac{1}{\Delta}\right)^{4-3d/2} (y_1 y_2 y_3)^{1-d/2}, \quad (18)$$

$s = (p_1 + p_2)^2$ and $\Delta = x_1 x_2 p_2^2/s + x_1 x_3 p_1^2/s + x_2 x_3$. Now, integration with respect to one of the Feynman parameters, say y_3 , can be performed trivially due to the δ function, leaving the integrations

$$\int_0^1 dy_1 \int_0^{1-y_1} dy_2 \cdots$$

Next, we perform the following change of variables

$$y_1 = 1 - \omega, \quad y_2 = \omega \rho \quad (19)$$

with the Jacobian being equal to ω . The resulting integral is over the unit square and the integration with respect to ω can be performed analytically, yielding the final result

$$T_I(A, B) = \frac{\Gamma(4-3d/2)}{\Gamma(2-d/2)^3} \frac{1-d/2}{16\pi \sin(d\pi/2)} \int_0^1 d\rho [(1-\rho)\rho]^{1-\frac{d}{2}} \left(\frac{1}{A\rho + B - B\rho}\right)^{4-\frac{3d}{2}} \times {}_2F_1\left[\frac{d}{2}, 4 - \frac{3d}{2}, 2, \frac{A\rho + B - B\rho + \rho(\rho-1)}{A\rho + B - B\rho}\right] \quad (20)$$

with ${}_2F_1$ being the hypergeometric function. The integrand is singular at both endpoints, but with an appropriate integration method, it can be integrated numerically. The result for three different values of d , i.e., 1.1, 1.5, and 1.9, are shown in Fig. 1, which were also calculated in Ref. [2] for $d = 1.1$ and $d = 1.9$. Just as in the case of the propagator, this is the exact three-point function (before coupling to the SM).

If one requires scale invariance only and not full conformal invariance of the hidden sector, the three-point function is not unique. Using self-couplings of continuous mass fields, it is possible to obtain nonunique three-point functions with simple expressions in momentum space [24]. However, because of the nonuniqueness of these three-point functions, this approach is less suitable for phenomenological studies.

Similarly, the four-point function has the general form [25, 26]

$$\langle \mathcal{O}_1(x_1)\mathcal{O}_2(x_2)\mathcal{O}_3(x_3)\mathcal{O}_4(x_4) \rangle = \rho \left(\frac{x_{12}^2 x_{34}^2}{x_{13}^2 x_{24}^2}, \frac{x_{12}^2 x_{34}^2}{x_{14}^2 x_{23}^2} \right) \prod_{i < j} (x_{ij}^2)^{\sum d_i/6 - (d_i + d_j)/2}, \quad (21)$$

for some function ρ that cannot be determined by conformal covariance alone. For a single field of scaling dimension d , one finds

$$\langle \mathcal{O}(x_1)\mathcal{O}(x_2)\mathcal{O}(x_3)\mathcal{O}^\dagger(x_4) \rangle = \frac{\rho' \left(\frac{x_{12}^2 x_{34}^2}{x_{13}^2 x_{24}^2}, \frac{x_{12}^2 x_{34}^2}{x_{14}^2 x_{23}^2} \right)}{(x_{13}^2)^d (x_{24}^2)^d}, \quad (22)$$

for ρ' related to ρ , which, in principle, can be used to study six-body final states. For this, one would have to assume a specific form of ρ' and then perform a Fourier transform of the result. This analysis, however, is beyond the scope of the present work.

IV. PHENOMENOLOGY

In this section, the main results of this work will be presented. These results will be based on an unparticle-induced effect qualitatively different from those of unparticle production and effects mediated through the propagator. This is the effect of unparticle *self-interactions*, first introduced by Feng, Rajaraman, and Tu [2], which for example can mediate processes with four-body final states at the LHC. While the authors of that paper considered the 4γ final state only and the experimental bound on the unparticle self-interaction strength using Tevatron data in the same channel, we will in this work consider also the $2\gamma 2\ell$ and 4ℓ final states at the LHC, including those final states in which two of the leptons are neutrinos. In

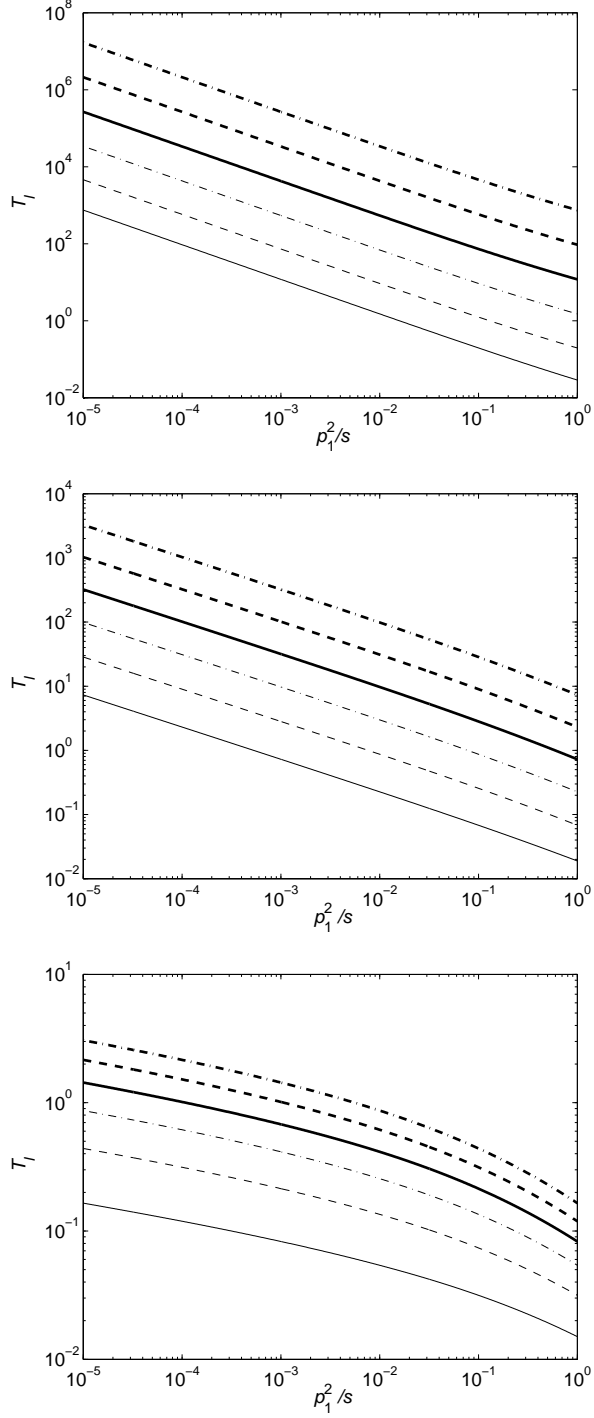


FIG. 1: The function $T_I(p_1^2/s, p_2^2/s)$ for $d = 1.1$ (top panel), $d = 1.5$ (middle panel), and $d = 1.9$ (bottom panel). The graphs are shown as a function of p_1^2/s for the following six discrete values: $p_2^2/s = 10^{-5}$ (thick, dash-dotted), 10^{-4} (thick, dashed), 10^{-3} (thick, solid), 10^{-2} (thin, dash-dotted), 10^{-1} (thin, dashed), and 1 (thin, solid).

addition, the 4ℓ channel at the Tevatron will be used to give more stringent bounds on the unparticle self-interaction strength and thus also on the LHC cross sections.

A. Unparticle Self-Interactions at the LHC

As discussed in Sec. III, three- and higher-point functions are in general nonvanishing in conformal field theories. These higher-point functions can mediate processes such as

$$\Omega\bar{\Omega} \rightarrow \mathcal{U} \rightarrow \mathcal{U}\cdots\mathcal{U},$$

where Ω is any SM particle, $\bar{\Omega}$ is its antiparticle, and the number of unparticles are two or more. If the conformal sector is strongly coupled, the creation of additional high-energy unparticles does not suppress the rate. This is in marked contrast to all SM processes where processes with additional high-energy particles are strongly suppressed.

The natural choice when dealing with these kinds of self-interactions is to concentrate on the effects of the three-point function. First, as discussed in Sec. III, the three-point function is completely specified up to an overall constant by conformal invariance, while the four- and higher-point functions are not. Second, this is the lowest order at which the resulting signal will have a strongly suppressed background. The unparticle three-point function can mediate processes such as

$$pp \rightarrow \mathcal{U} \rightarrow \mathcal{U}\mathcal{U} \rightarrow 4\gamma, 2\gamma 2\ell, 4\ell$$

and many others at the LHC. The basic parton-level Feynman diagrams are similar to the one shown in Fig. 2. The initial state can be either a gluon or a quark-antiquark pair, while the final state consists of two SM particle-antiparticle pairs, i.e., two of the pairs gg , $q\bar{q}$, W^+W^- , ZZ , $\gamma\gamma$, $\ell^+\ell^-$, $\nu\bar{\nu}$, and HH . In principle, one could also couple SM particles to one of the legs in the unparticle three-point function only, while amputating the other leg. The amputated three-point function has the form of the ordinary one, but with the amputated field replaced with its *conformal partner* with scaling dimension $4 - d$ [27]. This would lead to processes like

$$pp \rightarrow \mathcal{U} \rightarrow 2\gamma\mathcal{U}, 2\ell\mathcal{U}$$

with a phase space for two particles and one unparticle. Note that, although the addition of unparticle lines from higher-point functions leads to no suppression, coupling of these

to SM particles does lead to suppression simply because the particle-unparticle coupling is assumed to be small.

In producing the results of this work, the program CompHEP [28, 29] has been used. It includes the Monte Carlo integration algorithm VEGAS [30], which is used to integrate over phase space, and the CTEQ6L1 parton distribution functions (PDFs) [31]. No high-energy physics program that we are aware of has the ability to incorporate such a complicated momentum dependence as the one entering through the unparticle three-point function. Therefore, in order to use the user-friendly environment of CompHEP when performing phase space and PDF integrations, we have altered the C code to be able to enter the values of the three-point function. This makes it difficult to perform more complete simulations including the interference with SM diagrams and diagrams with one or two unparticle propagators. However, including the interference with SM diagrams will not be necessary at the Tevatron, since they are negligible (for the 4γ channel) or can be made so by imposing appropriate cuts (for the 4ℓ channel). This also means that the backgrounds will be unimportant at the LHC since the SM-unparticle couplings become more relevant at higher energies. If Λ_4 is larger than a few TeV or d is not very close to unity, inclusion of the diagrams with one or two unparticle propagators will also not be necessary. The reason is that a diagram with a single unparticle propagator contains two SM-unparticle couplings, and thus are suppressed by $1/\Lambda_4^{4d}$ in the cross section. In the same manner, two unparticle propagators means a $1/\Lambda_4^{8d}$ suppression. Of course, the contribution from the unparticle three-point function will be suppressed by $1/\Lambda_4^{6d}$, but this can be counteracted by potentially large values of C_d .

For leptons and photons in the final state, there are six different squared amplitudes, corresponding to the different subprocesses

$$gg, q\bar{q} \rightarrow \gamma\gamma\gamma\gamma, \gamma\gamma\ell\bar{\ell}, \ell_1\bar{\ell}_1\ell_2\bar{\ell}_2.$$

When calculating observables, the convention is to set $c_g = c_\gamma = 1$ and $e^2(c_4^f)^2 = 2\pi$ [11, 32]. In addition, following Ref. [2], $\Lambda_4 = 1$ TeV is chosen. This means that the only free parameters we have left are d and C_d .

It is worth emphasizing that there is no theoretical knowledge on what the values of C_d are in typical models of the unparticle sector. Also, there are no model independent bounds on C_d coming from more general considerations, although the authors of Ref. [33] believe their method could be used to derive such bounds. As will be shown, generation of the

relevant four-body final states requires $C_d \gg 1$. Because of the lack of knowledge on typical values of C_d , one cannot say if this makes it impossible to probe some models of the hidden sector through their self-interactions. In addition, if the relevant final states were to be observed at the LHC, this could not be used to extract any further information about the nature of hidden sector except the scaling dimension itself.

It is easy to observe that all cross sections will be proportional to C_d^2/Λ_4^{6d} and that the values of C_d and Λ_4 have no effect other than an overall factor in the cross sections. For numerical calculations, the value $C_d = 1$ is used and can then be given the appropriate value to yield the actual cross sections. Thus, the value of Λ_4 chosen has no effect on the total cross sections in the above processes if a change in Λ_4 can be accompanied by a change in the unparticle self-coupling constant C_d . However, this also means that an overall change of scale of the dimensionless couplings between the unparticle sector and the SM can be compensated by a change in C_d . For the sensitivity reach of the LHC on the unparticle couplings to photons and leptons, see e.g. Ref. [34]. Because of the unitarity bound $d \geq 1$ and the more practical bound $d < 2$, only this range on the scaling dimension is considered. More specifically, the values $d = 1.1, 1.5$, and 1.9 are used as representative values, hopefully giving a picture of the differences caused by the different scaling dimensions in the chosen range.

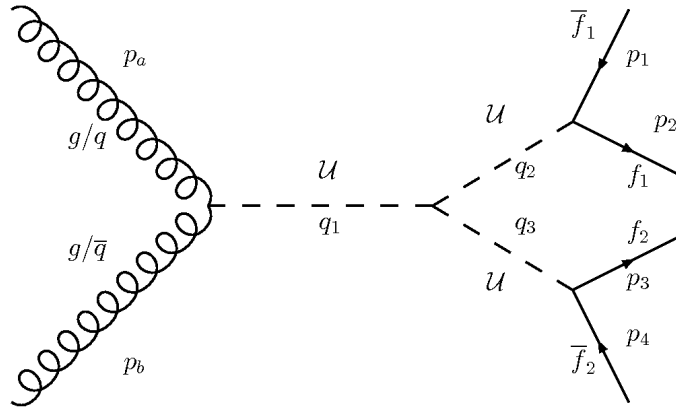


FIG. 2: The Feynman diagram for the subprocesses $gg/q\bar{q} \rightarrow \mathcal{U} \rightarrow \mathcal{U}\mathcal{U} \rightarrow f_1\bar{f}_1f_2\bar{f}_2$.

B. Four-Photon Final States

The four-photon final state mediated by unparticles has previously been studied in Ref. [2]. We include a similar analysis for completeness and also give distributions of invariant masses, which can be used to identify unparticles as the source as well as identify the scaling dimension. Using the Feynman rules given in Sec. II A, one finds that the squared amplitudes for the $gg \rightarrow 4\gamma$ and $q\bar{q} \rightarrow 4\gamma$ subprocesses are

$$\overline{|\mathcal{M}_{gg \rightarrow 4\gamma}|^2} = 2^{10} \frac{c_g^2 c_\gamma^4}{\Lambda_4^{6d}} (p_a \cdot p_b)^2 (p_1 \cdot p_2)^2 (p_3 \cdot p_4)^2 |\Gamma_3(q_2, q_3; d)|^2, \quad (23)$$

$$\overline{|\mathcal{M}_{q\bar{q} \rightarrow 4\gamma}|^2} = \frac{2^9 c_\gamma^4 e^2 (c_4^f)^2}{3 \Lambda_4^{6d}} v^2 (p_a \cdot p_b) (p_1 \cdot p_2)^2 (p_3 \cdot p_4)^2 |\Gamma_3(q_2, q_3; d)|^2, \quad (24)$$

respectively. These expressions do not include the factor of $1/4!$ needed to compensate for the overcounting caused by the integration over phase space for four identical particles. By dimensional analysis, the total partonic cross sections are given by

$$\hat{\sigma}(\hat{s})_{gg \rightarrow 4\gamma} = f_d^g C_d^2 \left(\frac{\hat{s}}{\Lambda_4^2} \right)^{3d} \frac{1}{\hat{s}/\text{GeV}^2} \text{fb}, \quad (25)$$

$$\hat{\sigma}(\hat{s})_{q\bar{q} \rightarrow 4\gamma} = f_d^q C_d^2 \left(\frac{\hat{s}}{\Lambda_4^2} \right)^{3d} \frac{v^2}{\hat{s}} \frac{1}{\hat{s}/\text{GeV}^2} \text{fb}, \quad (26)$$

where f_d^g and f_d^q are dimensionless numbers, which can be extracted from the Monte Carlo integration and are listed in Table I for different values of d .

The final state photons are required to satisfy the conditions³

$$p_T^i > 15 \text{ GeV}, \quad |\eta^i| < 2.5 \quad (27)$$

with p_T^i and η^i being the transverse momentum and the rapidity of the i -th photon, respectively, and $i = 1, 2, 3, 4$. The resulting reference cross sections $\sigma_{gg/q\bar{q} \rightarrow 4\gamma}^{\text{LHC,ref}}$ (i.e., using $C_d = 1$) at the LHC with $\sqrt{s} = 14 \text{ TeV}$ are presented in Table I. Note that our cross sections differ slightly from the results presented in Ref. [2], which is most likely due to different parton distribution functions. As argued in Sec. IV E, Tevatron measurements give constraints on C_d . Multiplying the sum of the reference cross sections by this number squared, yields upper bounds on the LHC cross sections, $\sigma_{4\gamma}^{\text{LHC,max}}$, which can also be found in Table I. The

³ All photons have transverse momenta well above 15 GeV. Thus, imposing slightly harder p_T -cuts will have no effect on the signal.

allowed cross sections are observed to depend strongly on d , from only 6.0 fb for $d = 1.1$ to $1.2 \cdot 10^6$ fb for $d = 1.9$.

We have also generated a large number of events, enabling the calculation of different distributions. In Fig. 3, the distribution of the two-body invariant photon masses $m_{ij} = \sqrt{(p_i + p_j)^2}$ are shown. Since there are six different ways of combining four identical particles, each event will contribute six counts. In Fig. 4, the distribution of the full four-body invariant mass $m_{4\gamma} = \sqrt{(p_1 + p_2 + p_3 + p_4)^2}$ is shown. These spectra are presented for the gg initial state only, which dominate at the LHC. However, after having generated spectra for a sample of $q\bar{q}$ initial states and different values of d , one finds almost perfect agreement with the spectra for the gg initial state. Thus, if for some reason the unparticle field does not couple to gluons at all, the resulting spectra would be virtually identical although the total cross sections would be different. What is evident is, first of all, the absence of any resonance, owing to the scale-invariant nature of the unparticle sector. Second, these distributions depend very strongly on the unparticle scaling dimension. This is a general property of all the spectra presented in this work; they all become very much softer when d decreases from 1.9 to 1.1.

The SM background consists mainly of direct diphoton production with two photons attached to the quark lines. With the same cuts as above, we find the SM background to be approximately 0.1 fb. Obviously, if the unparticle cross sections are anywhere near the values allowed by Tevatron data, there is no need to consider the interference effects with the SM. Thus, if there was to be an excess of 4γ events at the LHC, the given distributions could possibly be used to identify unparticles as the source, as well as the correct value of the scaling dimension d . Since there is no distinction between the couplings to photons and gluons, the distributions of gluons in the $4g$ and $2g2\gamma$ channels would be identical. Although the total cross section will be larger in this case due to the multiple colors of the gluons, the large QCD background will make the observation in this channel more difficult.

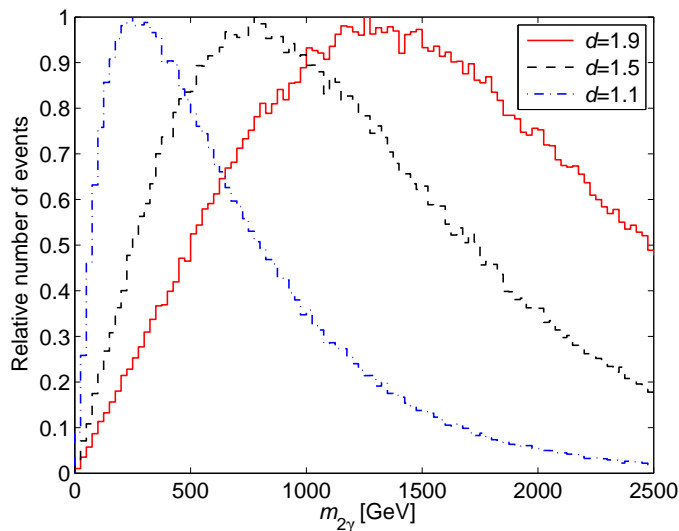


FIG. 3: The distributions of photon two-body invariant masses in unparticle-mediated 4γ events at the LHC for three different values of the scaling dimension $d = 1.9$ (red solid curve), $d = 1.5$ (black dashed curve), and $d = 1.1$ (blue dashed-dotted curve). The bin width used is 25 GeV. Note that each event contributes six counts.

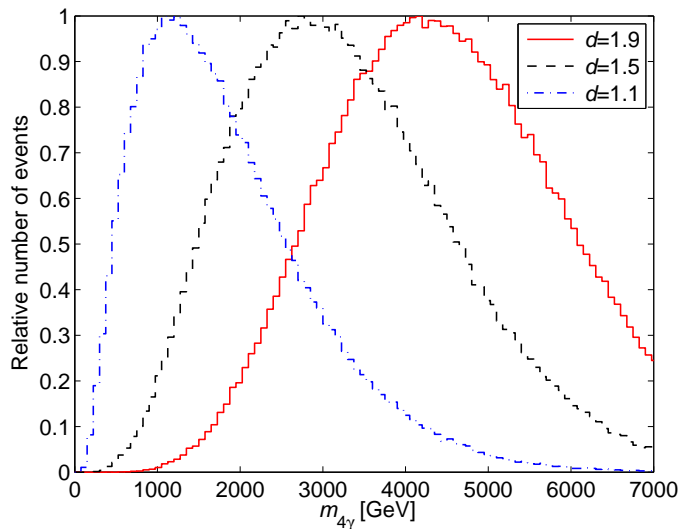


FIG. 4: The distributions of photon four-body invariant masses in unparticle-mediated 4γ events at the LHC for three different values of the scaling dimension $d = 1.9$ (red solid curve), $d = 1.5$ (black dashed curve), and $d = 1.1$ (blue dashed-dotted curve). The bin width used is 75 GeV.

	$d = 1.1$	$d = 1.5$	$d = 1.9$
f_d^g	3.0	0.17	0.021
f_d^q	6.3	0.35	0.044
h_d^g	790	16	1.6
h_d^q	$1.7 \cdot 10^3$	34	3.3
j_d^g	$1.3 \cdot 10^4$	160	14
j_d^q	$2.8 \cdot 10^4$	330	29
Combined 4γ and 4ℓ bound on C_d	450	$1.8 \cdot 10^4$	$1.9 \cdot 10^5$
$\sigma_{gg \rightarrow 4\gamma}^{\text{LHC,ref}}$ [fb]	$2.9 \cdot 10^{-5}$	$1.1 \cdot 10^{-5}$	$3.2 \cdot 10^{-5}$
$\sigma_{q\bar{q} \rightarrow 4\gamma}^{\text{LHC,ref}}$ [fb]	$1.0 \cdot 10^{-6}$	$3.8 \cdot 10^{-7}$	$1.1 \cdot 10^{-6}$
$\sigma_{4\gamma}^{\text{LHC,max}}$ [fb]	6.0	$3.7 \cdot 10^3$	$1.2 \cdot 10^6$
$\sigma_{gg \rightarrow 2\gamma 2\ell}^{\text{LHC,ref}}$ [fb]	$3.8 \cdot 10^{-4}$	$1.1 \cdot 10^{-5}$	$1.0 \cdot 10^{-5}$
$\sigma_{q\bar{q} \rightarrow 2\gamma 2\ell}^{\text{LHC,ref}}$ [fb]	$2.0 \cdot 10^{-5}$	$4.0 \cdot 10^{-7}$	$3.7 \cdot 10^{-7}$
$\sigma_{2\gamma 2\ell}^{\text{LHC,max}}$ [fb]	81	$3.7 \cdot 10^3$	$3.7 \cdot 10^5$
$\sigma_{gg \rightarrow 2e 2\mu}^{\text{LHC,ref}}$ [fb]	$2.6 \cdot 10^{-3}$	$4.6 \cdot 10^{-6}$	$7.7 \cdot 10^{-7}$
$\sigma_{q\bar{q} \rightarrow 2e 2\mu}^{\text{LHC,ref}}$ [fb]	$2.7 \cdot 10^{-4}$	$2.2 \cdot 10^{-7}$	$2.6 \cdot 10^{-8}$
$\sigma_{2e 2\mu}^{\text{LHC,max}}$ [fb]	580	$1.6 \cdot 10^3$	$2.9 \cdot 10^4$

TABLE I: The dimensionless constants $f_d^{g,q}$, $h_d^{g,q}$, and $j_d^{g,q}$, appearing in the partonic cross sections, as well as the unparticle 4γ , $2\gamma 2\ell$, and $2e 2\mu$ reference cross sections at the LHC for $d = 1.1, 1.5$, and 1.9 . The reference cross sections are calculated with $C_d = 1$, while the actual cross sections are proportional to C_d^2 , which is bounded by Tevatron data (see Sec. IV E), giving upper bounds on total cross sections for all final states at the LHC.

C. Two-Photon and Two-Lepton Final States

Simply replacing two of the photons with one charged lepton-antilepton pair, yields the subprocesses $gg \rightarrow 2\gamma 2\ell$ and $q\bar{q} \rightarrow 2\gamma 2\ell$ with squared amplitudes

$$\overline{|\mathcal{M}_{gg \rightarrow 2\gamma 2\ell}|^2} = 64 \frac{c_\gamma^2 c_g^2 e^2 (c_4^f)^2}{\Lambda_4^{6d}} v^2 (p_a \cdot p_b)^2 (p_1 \cdot p_2)^2 (p_3 \cdot p_4) |\Gamma_3(q_2, q_3; d)|^2, \quad (28)$$

$$\overline{|\mathcal{M}_{q\bar{q} \rightarrow 2\gamma 2\ell}|^2} = \frac{32}{3} \frac{c_\gamma^2 e^4 (c_4^f)^4}{\Lambda_4^{6d}} v^4 (p_a \cdot p_b) (p_1 \cdot p_2)^2 (p_3 \cdot p_4) |\Gamma_3(q_2, q_3; d)|^2, \quad (29)$$

respectively. These expressions should be multiplied with $1/2!$ to account for the identical photons in the final state. Just as in the four-photon case, the partonic cross sections can be written as

$$\hat{\sigma}(\hat{s})_{gg \rightarrow 2\gamma 2\ell} = h_d^g C_d^2 \left(\frac{\hat{s}}{\Lambda_4^2} \right)^{3d} \frac{v^2}{\hat{s}} \frac{1}{\hat{s}/\text{GeV}^2} \text{fb}, \quad (30)$$

$$\hat{\sigma}(\hat{s})_{q\bar{q} \rightarrow 2\gamma 2\ell} = h_d^q C_d^2 \left(\frac{\hat{s}}{\Lambda_4^2} \right)^{3d} \left(\frac{v^2}{\hat{s}} \right)^2 \frac{1}{\hat{s}/\text{GeV}^2} \text{fb}, \quad (31)$$

where the proportionality factors are again listed in Table I. The same procedure as in the four-photon case also yields the reference and maximum cross sections at the LHC, where the same single-particle cuts have been imposed. The allowed cross sections are of the same order of magnitude as the 4γ channel, although the difference between different values of the scaling dimension is now smaller. Still, there is the possibility to have very large cross sections for large d .

The p_T distributions of the photon with the highest transverse momentum and the distribution of the charged lepton invariant masses are shown in Figs. 5 and 6, respectively. Again, one observes the dramatic softening of the distributions as the scaling dimension decreases and just as in the four-photon case, almost perfect agreement between the distributions from the gg and $q\bar{q}$ initial states are found.

Using CompHEP, the SM cross section is calculated to be of the order of 30 fb per lepton flavor. There will be resonances at charged lepton invariant masses 0 and $M_Z \simeq 90$ GeV. Thus, we demand that the charged lepton invariant masses exceed 110 GeV, which yields a reduction of the cross section to approximately 1 fb. As can be observed from Fig. 6, this cut will have a very small effect on the signal, especially for d not very close to unity. Accordingly, the SM backgrounds will be negligible for C_d anywhere close to its allowed values. In analogy with the four-photon case, since the unparticle field is assumed to couple

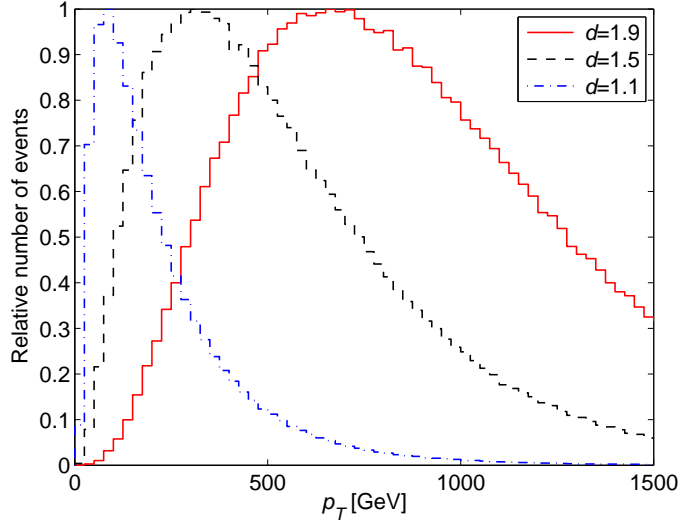


FIG. 5: The p_T distributions of the highest- p_T photon in unparticle-mediated $2\gamma 2\ell$ events at the LHC for three different values of the scaling dimension $d = 1.9$ (red solid curve), $d = 1.5$ (black dashed curve), and $d = 1.1$ (blue dashed-dotted curve). The bin width used is 25 GeV.

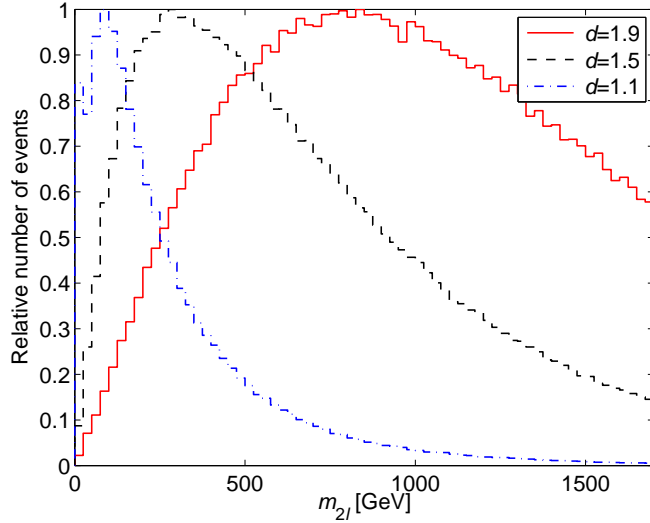


FIG. 6: The distributions of the charged lepton invariant masses in unparticle-mediated $2\gamma 2\ell$ events at the LHC for three different values of the scaling dimension $d = 1.9$ (red solid curve), $d = 1.5$ (black dashed curve), and $d = 1.1$ (blue dashed-dotted curve). The bin width used is 25 GeV.

to quarks and gluons, one should also find $q\bar{q}gg$, $q\bar{q}\gamma\gamma$, and $\ell\bar{\ell}gg$ final states with identical spectra, but larger cross sections.

D. Four-Charged Lepton Final States

For four charged leptons in the final state, the squared amplitudes are given by

$$\overline{|\mathcal{M}_{gg \rightarrow 4\ell}|^2} = 4 \frac{c_g^2 e^4 (c_4^f)^4}{\Lambda_4^{6d}} v^4 (p_a \cdot p_b)^2 (p_1 \cdot p_2)(p_3 \cdot p_4) |\Gamma_3(q_2, q_3; d)|^2, \quad (32)$$

$$\overline{|\mathcal{M}_{q\bar{q} \rightarrow 4\ell}|^2} = \frac{2}{3} \frac{e^6 (c_4^f)^6}{\Lambda_4^{6d}} v^6 (p_a \cdot p_b)(p_1 \cdot p_2)(p_3 \cdot p_4) |\Gamma_3(q_2, q_3; d)|^2, \quad (33)$$

respectively. The relevant final states are $4e$, 4μ and $2e2\mu$. The cross sections can again be found in Table I and are given for the $2e2\mu$ final state. Similar to the previous final states, the partonic cross sections are

$$\hat{\sigma}(\hat{s})_{gg \rightarrow 4\ell} = j_d^g C_d^2 \left(\frac{\hat{s}}{\Lambda_4^2} \right)^{3d} \left(\frac{v^2}{\hat{s}} \right)^2 \frac{1}{\hat{s}/\text{GeV}^2} \text{fb}, \quad (34)$$

$$\hat{\sigma}(\hat{s})_{q\bar{q} \rightarrow 4\ell} = j_d^q C_d^2 \left(\frac{\hat{s}}{\Lambda_4^2} \right)^{3d} \left(\frac{v^2}{\hat{s}} \right)^3 \frac{1}{\hat{s}/\text{GeV}^2} \text{fb}. \quad (35)$$

In Fig. 7, the p_T distributions of the highest- p_T lepton are shown, while Fig. 8 depicts the distribution of the invariant masses of three leptons of which two have the same charge. Since there are two ways of combining three leptons, each event will contribute two counts. Again, there is a strong dependence on d .

The four-charged lepton channel is a very clean and important channel when it comes to the discovery potential of the Higgs boson ($H \rightarrow ZZ \rightarrow 4\ell$) at the LHC. Thus, one can compare the cross sections originating from the unparticle self-interactions to the already existing calculated backgrounds in connection with the Higgs boson [35, 36]. With the cuts $p_T > 5$ GeV and $|\eta| < 2.5$, the irreducible background is about 70 fb, coming mainly from two Z -bosons decaying into four charged leptons. Furthermore, with cuts on the invariant masses of the charged leptons, it should be easy to reduce this part of the background to a few fb. The reducible backgrounds stem from the $t\bar{t} \rightarrow W^+bW^-\bar{b} \rightarrow 4\ell + X$ and $Zb\bar{b} \rightarrow 4\ell + X$ processes with a cross section of $7.0 \cdot 10^3$ fb. Since the events coming from these processes contain b jets in the final state, they can be reduced below the irreducible levels, using cuts on the track isolation and impact parameters without significant reduction of the signal. Thus, the possible cross sections from unparticles summed over all channels, 10^3 fb – 10^5 fb, are potentially huge compared to the backgrounds.

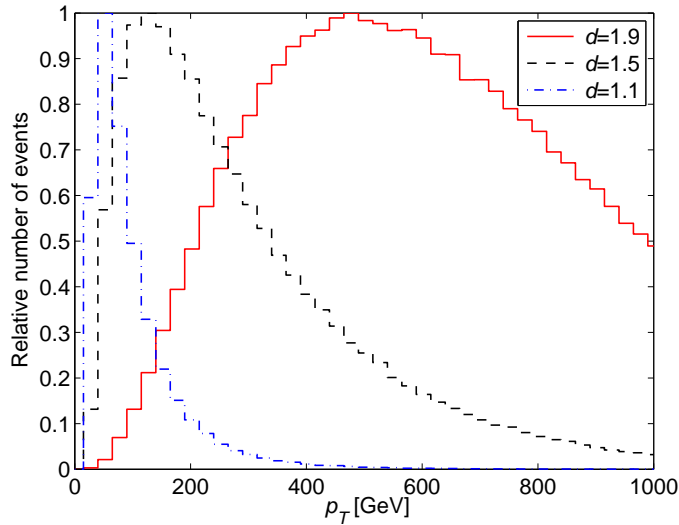


FIG. 7: The p_T -distributions of the highest- p_T lepton in unparticle-mediated 4ℓ events at the LHC for three different values of the scaling dimension $d = 1.9$ (red solid curve), $d = 1.5$ (black dashed curve), and $d = 1.1$ (blue dashed-dotted curve). The bin width used is 25 GeV.

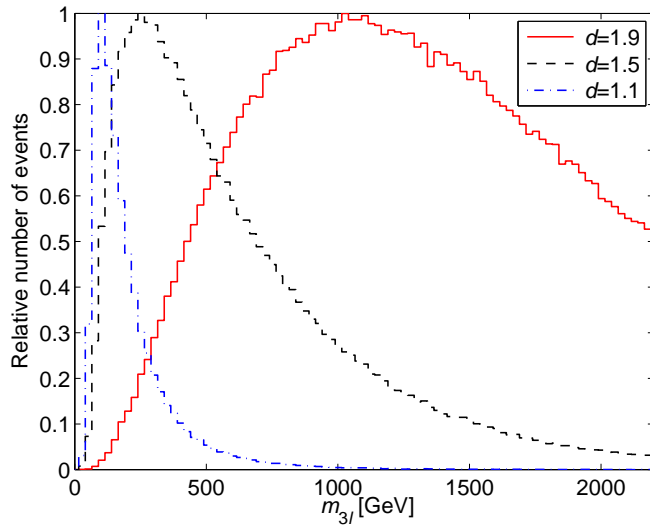


FIG. 8: The distributions of the three-body invariant lepton masses in unparticle-mediated 4ℓ events at the LHC for three different values of the scaling dimension $d = 1.9$ (red solid curve), $d = 1.5$ (black dashed curve), and $d = 1.1$ (blue dashed-dotted curve). The bin width used is 25 GeV. Note that each event contributes two counts.

E. Tevatron Bounds

In order to give bounds on the cross sections of processes mediated by unparticle self-interactions, one needs bounds on the constant C_d appearing in the three-point function in Eq. (17), which determines the strength of the self-interaction. However, there is no known way to bound C_d theoretically, and thus, one needs to turn to experiments. These bounds could come from many different experiments. Since unparticle effects are most easily probed at high-energy colliders and there are no LHC data available yet, it is natural to turn to the existing Tevatron data. It is important to remember that these bounds, and hence, the bounds on the LHC cross sections, depend on the values given to the dimensionless coupling constants between the SM and unparticle fields. For example, if the unparticle field does not couple to gluons at all, the allowed cross section at the LHC will be smaller, since the gg initial state is dominating at the LHC, while the $q\bar{q}$ initial state is dominating at the Tevatron.

1. The 4γ channel

In this section, we repeat the analysis performed in Ref. [2], but find less stringent constraints on C_d . This is because we find smaller cross sections⁴ and we take into account the single photon detection efficiency.

The SM background at the Tevatron is calculated to be approximately 0.01 fb. Using 0.83 fb⁻¹ of data, the D0 Collaboration found no candidate events [37]. Thus, the 95 % C.L. bound equal to three on the mean of a Poisson process [38] becomes the bound on C_d

$$C_d^2 < \frac{3}{0.83 \text{ fb}^{-1} \sigma_{4\gamma}^{\text{Tev,ref}} \epsilon_\gamma^4},$$

where $\sigma_{4\gamma}^{\text{Tev,ref}}$ is the total reference cross section at the Tevatron and $\epsilon_\gamma = 0.9$ is taken as the single photon detection efficiency. The values of $\sigma_{4\gamma}^{\text{Tev,ref}}$ and the bounds on C_d can be found in Table II. These bounds are approximately 4 times less restrictive in terms of cross sections than the bounds found in Ref. [2]. However, this does not matter, since the bounds from the 4ℓ channel calculated in Sec. IV E 2 will be even more restrictive.

⁴ However, the cross sections are almost identical to the ones in Ref. [2] when we remove all our cuts.

	$d = 1.1$	$d = 1.5$	$d = 1.9$
$\sigma_{4\gamma}^{\text{Tev,ref}}$ [fb]	$8.5 \cdot 10^{-9}$	$1.0 \cdot 10^{-10}$	$6.1 \cdot 10^{-12}$
Bounds on C_d	$2.6 \cdot 10^4$	$2.3 \cdot 10^5$	$9.5 \cdot 10^5$

TABLE II: The Tevatron reference cross sections in the 4γ channel and the resulting upper bounds on C_d .

2. The 4ℓ channel

The D0 Collaboration has also searched for four-charged lepton final states [39–41] with an approximate integrated luminosity of 1 fb^{-1} in all channels. Since electrons and muons are detected in different ways in the detector, one needs to separate their analyses.

For the 4μ channel, the relevant geometric cut is $|\eta| < 2$ and the kinematical ones are $p_T > 15 \text{ GeV}$ and $\cos \alpha_i < 0.96$, where the α_i 's are the angles between all six muon pairs. Also, the two invariant masses of the muon pairs in at least one of three possible pairings must both be larger than 30 GeV . In addition, there are losses in acceptances due to the requirement on having a track match, the quality of the signal of the detected muons, and the efficiencies of the triggers. We implement the cuts on η , p_T , $\cos \alpha_i$ and also the more conservative demand that the invariant masses of $M_{12} = \sqrt{(p_1 + p_2)^2}$ and $M_{34} = \sqrt{(p_3 + p_4)^2}$ are both larger than 30 GeV . To eliminate the SM background, which is dominated by the intermediate states with two Z bosons or photons, the additional cut $M_{12}, M_{34} \notin [M_Z - 4\Gamma_Z, M_Z + 4\Gamma_Z] = [81.2 \text{ GeV}, 101.2 \text{ GeV}]$ is imposed. We approximate the acceptances for the track match, detector quality cuts, and trigger efficiencies to be the same as for the ZZ intermediate state in Refs. [39–41], giving a total acceptance loss of approximately $\epsilon_{4\ell} = 0.5$.

In the $4e$ channel, the same requirements on p_T and the invariant masses are applied. However, the rapidity cuts for electrons are instead $|\eta| < 1.1$ or $1.5 < |\eta| < 3.2$. The spatial separation $R = \sqrt{(\eta_i - \eta_j)^2 + (\phi_i - \phi_j)^2}$ is required to be larger than 0.4 . In the same way as for the 4μ channel, the additional acceptance loss is approximated to be 0.5 from the cut on R , the electron quality cuts, and the efficiencies of the triggers.

Finally, for the $2e2\mu$ channel, the same single-particle cuts as in the $4e$ and 4μ channels are applied. Here $\cos \alpha < 0.96$ for the two muons and $R > 0.2$ for all the final state particles.

The same procedure for the $4e$ channel yields an additional acceptance loss of 0.5.

The SM background is now approximately zero and no events with our requirements on the invariant masses were found. Thus, we obtain the 95 % C.L. bound on C_d

$$C_d^2 < \frac{3}{1 \text{ fb}^{-1} \epsilon_{4\ell} \left(\sigma_{4e}^{\text{Tev,ref}} + \sigma_{4\mu}^{\text{Tev,ref}} + \sigma_{2e2\mu}^{\text{Tev,ref}} \right)}.$$

The cross section in each channel and the calculated upper bounds on C_d can be found in Table III. One observes that the bounds from the 4ℓ channels are about $3.3 \cdot 10^3$, 160, and 25 times more severe than the ones from the 4γ channel in terms of cross sections for $d = 1.1, 1.5$, and 1.9 , respectively. Thus, the 4ℓ final states produce more restrictive upper bounds on the cross sections than the 4γ final states. In conclusion, this means that the upper bounds on the cross sections from the 4ℓ final states should replace the ones obtained earlier in the literature [2].

	$d = 1.1$	$d = 1.5$	$d = 1.9$
$\sigma_{4\mu}^{\text{Tev,ref}}$ [fb]	$4.6 \cdot 10^{-6}$	$4.7 \cdot 10^{-9}$	$4.4 \cdot 10^{-11}$
$\sigma_{4e}^{\text{Tev,ref}}$ [fb]	$3.9 \cdot 10^{-6}$	$1.8 \cdot 10^{-9}$	$1.8 \cdot 10^{-11}$
$\sigma_{2e2\mu}^{\text{Tev,ref}}$ [fb]	$2.1 \cdot 10^{-5}$	$1.2 \cdot 10^{-8}$	$1.1 \cdot 10^{-10}$
Bounds on C_d	450	$1.8 \cdot 10^4$	$1.9 \cdot 10^5$

TABLE III: The Tevatron reference cross sections in the 4ℓ channels and the calculated upper bounds on C_d .

F. Missing Transverse Momentum

The couplings of SM neutrinos to a scalar unparticle field are usually taken as [42–45]

$$\frac{\lambda^{\alpha\beta}}{\Lambda_3^{d-1}} \bar{\nu}_\alpha \nu_\beta \mathcal{O}_U, \quad (36)$$

where $\alpha, \beta = e, \mu, \tau$ are flavor indices. For flavor conserving couplings, the matrix $\lambda = (\lambda^{\alpha\beta})$ is, of course, diagonal. This can lead to the decay of heavy neutrinos to lighter ones [42] and other interesting phenomenological consequences. Here, however, the focus will be on processes such as

$$pp \rightarrow 2\gamma\nu\bar{\nu}, 2\ell\nu\bar{\nu}.$$

The couplings in Eq. (36) will lead to the same squared amplitudes as given in Eqs. (28) and (32), up to an overall factor.

One cannot say anything about the total cross sections for these kinds of processes unless one has knowledge about the couplings $\lambda^{\alpha\beta}$. For $\lambda^{\alpha\beta}$ of the order of unity and Λ_3 of the order of 1 TeV, the resulting cross sections would be of the same order of magnitude as the ones calculated for the $2\gamma 2\ell$ and 4ℓ channels in Secs. IV C and IV D, respectively. The distributions of missing transverse momentum, \cancel{p}_T , for $2\gamma 2\nu$ and $2\ell 2\nu$ events at the LHC are shown in Figs. 9 and 10, respectively. Compared with the events expected from SM processes [46, 47], the events mediated by unparticles are observed to contain large \cancel{p}_T , especially for larger values of d . In addition, since the total rates could be relatively large, a high cut on \cancel{p}_T could be used to search for unparticle physics in the $2\gamma + \cancel{p}_T$ and $2\ell + \cancel{p}_T$ channels as well.

V. SUMMARY AND CONCLUSIONS

Unparticle physics is a relatively new idea for an extension of the SM of particle physics, introduced by Georgi in 2007 [1]. The basic idea is that there might exist a hidden conformal sector, which is coupled to the SM through effective operators. Thus, unparticle physics is the study of the phenomenological consequences of the SM interactions with such a hidden sector.

In this work, the implications of the unparticle self-interactions, entering through the three-point correlation function, for LHC phenomenology have been investigated. For weak enough couplings of the unparticle sector to the SM, i.e., for a high enough unparticle scale Λ_4 , unparticle physics will be impossible to observe in all previously studied processes, i.e., those including unparticle propagators and external lines. Because of the new degree of freedom entering through the self-interactions, this does not necessarily apply to the processes studied in this work, assuming large values of C_d are allowed. Thus, it is not only possible that these processes could be used as a favorable way to look for unparticle physics, but also that it might be the only way.

The final states examined were the 4γ , $2\gamma 2\ell$, and 4ℓ final states, the first of which has been studied previously in the literature [2]. In addition, we have used the analysis of the 4ℓ channel at the Tevatron to calculate constraints on the constant appearing in the unparticle three-point correlation function, enabling determination of the maximum allowed

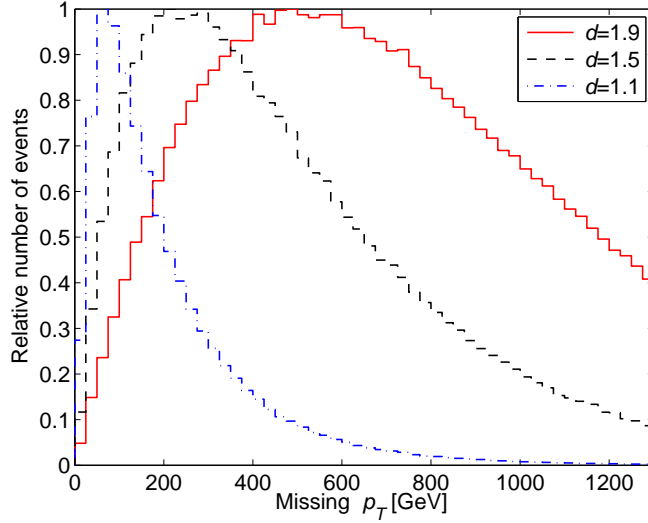


FIG. 9: The missing transverse momentum in unparticle-mediated $2\gamma\nu\bar{\nu}$ events at the LHC for three different values of the scaling dimension $d = 1.9$ (red solid curve), $d = 1.5$ (black dashed curve), and $d = 1.1$ (blue dashed-dotted curve). The bin width used is 25 GeV.

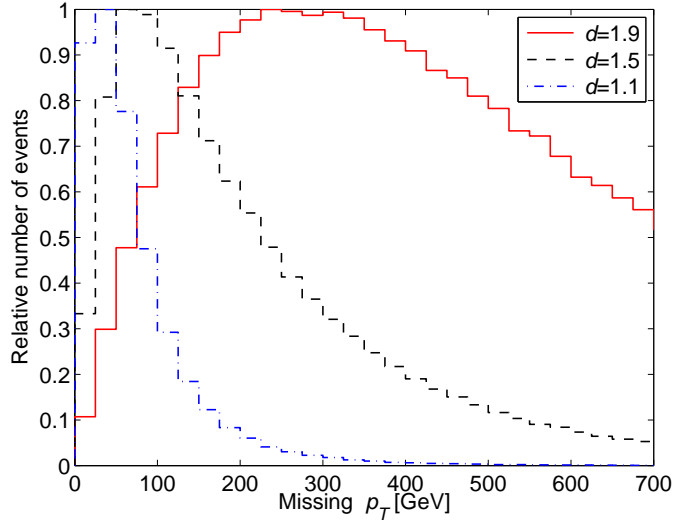


FIG. 10: The missing transverse momentum in unparticle-mediated $2\ell\nu\bar{\nu}$ events at the LHC for three different values of the scaling dimension $d = 1.9$ (red solid curve), $d = 1.5$ (black dashed curve), and $d = 1.1$ (blue dashed-dotted curve). The bin width used is 25 GeV. Note the different scale on the p_T axis as compared to Fig. 9.

cross sections at the LHC. The results take the form of upper bounds on the LHC cross sections and distributions of transverse momenta, invariant masses, and missing transverse

momenta.

The allowed cross sections have been found to depend strongly on the scaling dimension d of the unparticle sector. In general, they are much smaller for d close to 1 and increase as d increases towards 2 in which case the cross section can be as large as 10^6 fb. For $d = 1.9$, we obtained 10^6 fb for the 4γ final state, 10^5 fb for each of the the $2\gamma 2\ell$ final states, and 10^4 fb for each of the 4ℓ final states. However, for smaller values of d , the allowed cross sections are much smaller due to our new constraints from the 4ℓ channel at the Tevatron, which are indeed much stronger and replace the upper bounds from the 4γ channel. In addition, the calculated distributions have been observed to depend strongly on the scaling dimension and become much softer when it decreases towards 1. Finally, if there was to be an excess of events of the relevant final states at the LHC (possibly enormous), unparticle physics would be one possible description. The computed distributions could then potentially be used to identify unparticles as the source, as well as the correct value of the scaling dimension d .

Acknowledgments

We would like to thank Chad Jarvis and He Zhang for useful discussions. This work was supported by the Royal Swedish Academy of Sciences (KVA) [T.O.] and the Swedish Research Council (Vetenskapsrådet), contract nos. 621-2005-3588 and 621-2008-4210 [T.O.]

-
- [1] H. Georgi, Phys. Rev. Lett. **98**, 221601 (2007), hep-ph/0703260.
 - [2] J. L. Feng, A. Rajaraman, and H. Tu, Phys. Rev. **D77**, 075007 (2008), 0801.1534.
 - [3] M. J. Strassler (2008), 0801.0629.
 - [4] H. Georgi and Y. Kats (2009), 0904.1962.
 - [5] T. Banks and A. Zaks, Nucl. Phys. **B196**, 189 (1982).
 - [6] T. A. Ryttov and F. Sannino, Phys. Rev. **D76**, 105004 (2007), 0707.3166.
 - [7] B. Grinstein, K. A. Intriligator, and I. Z. Rothstein, Phys. Lett. **B662**, 367 (2008), 0801.1140.
 - [8] J. Polchinski, Nucl. Phys. **B303**, 226 (1988).
 - [9] Y. Nakayama, Phys. Rev. **D76**, 105009 (2007), 0707.2451.
 - [10] G. Mack, Commun. Math. Phys. **55**, 1 (1977).

- [11] M. Bander, J. L. Feng, A. Rajaraman, and Y. Shirman, Phys. Rev. **D76**, 115002 (2007), 0706.2677.
- [12] P. J. Fox, A. Rajaraman, and Y. Shirman, Phys. Rev. **D76**, 075004 (2007), 0705.3092.
- [13] K. Cheung, W.-Y. Keung, and T.-C. Yuan, Phys. Rev. **D76**, 055003 (2007), 0706.3155.
- [14] K. Cheung, W.-Y. Keung, and T.-C. Yuan, Phys. Rev. Lett. **99**, 051803 (2007), 0704.2588.
- [15] H. Georgi, Phys. Lett. **B650**, 275 (2007), 0704.2457.
- [16] G. Cacciapaglia, G. Marandella, and J. Terning, JHEP **01**, 070 (2008), 0708.0005.
- [17] A. Rajaraman, AIP Conf. Proc. **1078**, 63 (2008), 0809.5092.
- [18] A. Rajaraman, Phys. Lett. **B671**, 411 (2009), 0806.1533.
- [19] A. Delgado, J. R. Espinosa, J. M. No, and M. Quiros, Phys. Rev. **D79**, 055011 (2009), 0812.1170.
- [20] K. Cheung, W.-Y. Keung, and T.-C. Yuan, AIP Conf. Proc. **1078**, 156 (2008), 0809.0995.
- [21] S.-L. Chen and X.-G. He, Phys. Rev. **D76**, 091702 (2007), 0705.3946.
- [22] G. von Gersdorff and M. Quiros, Phys. Lett. **B678**, 317 (2009), 0901.0006.
- [23] H. Osborn and A. C. Petkou, Ann. Phys. **231**, 311 (1994), hep-th/9307010.
- [24] N. G. Deshpande and H. Xiao-Gang, Phys. Rev. **D78**, 055006 (2008), 0806.2009.
- [25] P. H. Ginsparg (1988), hep-th/9108028.
- [26] P. Di Francesco, P. Mathieu, and D. Senechal, *Conformal Field Theory* (Springer, New York, USA, 1997).
- [27] I. Mitra (2009), 0907.1769.
- [28] E. Boos et al. (CompHEP), Nucl. Instrum. Meth. **A534**, 250 (2004), hep-ph/0403113.
- [29] A. Pukhov et al. (1999), hep-ph/9908288.
- [30] G. P. Lepage, J. Comput. Phys. **27**, 192 (1978).
- [31] J. Pumplin et al., JHEP **07**, 012 (2002), hep-ph/0201195.
- [32] E. Eichten, K. D. Lane, and M. E. Peskin, Phys. Rev. Lett. **50**, 811 (1983).
- [33] V. S. Rychkov and A. Vichi, Phys. Rev. **D80**, 045006 (2009), 0905.2211.
- [34] I. Sahin and S. C. Inan (2009), JHEP **09**, 069 (2009), 0907.3290.
- [35] ATLAS Collaboration (2008), ATL-PHYS-CONF-2008-013.
- [36] ATLAS Collaboration (2008), ATL-PHYS-PROC-2008-045.
- [37] DØ Collaboration (2007), DØ Note 5067-CONF.
- [38] G. J. Feldman and R. D. Cousins, Phys. Rev. **D57**, 3873 (1998), physics/9711021.

- [39] V. M. Abazov et al. (DØ Collaboration), Phys. Rev. Lett. **100**, 131801 (2008), 0712.0599.
- [40] C. R. Jarvis (2007), FERMILAB-THESIS-2007-54.
- [41] DØ Collaboration (2007), DØ Note 5345-CONF.
- [42] S. Zhou, Phys. Lett. **B659**, 336 (2008), 0706.0302.
- [43] J. Barranco, A. Bolanos, O. G. Miranda, C. A. Moura, and T. I. Rashba, Phys. Rev. **D79**, 073011 (2009), 0901.2099.
- [44] D. Montanino, M. Picariello, and J. Pulido, Phys. Rev. **D77**, 093011 (2008), 0801.2643.
- [45] A. B. Balantekin and K. O. Ozansoy, Phys. Rev. **D76**, 095014 (2007), 0710.0028.
- [46] ATLAS Collaboration (2004), ATL-PHYS-2004-028.
- [47] ATLAS Collaboration (2009), ATL-PHYS-PUB-2009-086.